Supporting information

Unusual O^{2-}/F^{-} distribution in the new pyrochlore oxyfluorides: $Na_2B_2O_5F_2$ (B= Nb, Ta).

Edouard Boivin[a,*], Frédérique Pourpoint[a], Sébastien Saitzek[a], Pardis Simon[a], Pascal Roussel[a], Houria Kabbour[a,*]

a. *Univ. Lille, CNRS, Centrale Lille, ENSCL, Univ. Artois, UMR 8181-UCCS-Unité de Catalyse et Chimie du Solide, F-59000 Lille, France.*

Experimental and computational methods

Approximatively 1g of sample is synthetized from, Nb_2O_5 (Sigma-Aldrich, 99.9%) or Ta_2O_5 (Sigma-Aldrich, 99.9%) in 15 mL of a NaF (Sigma-Aldrich, >99%) aqueous solution (0.02 M) under hydrothermal conditions in a 23 mL vessel (approximately 2/3 filled) at 240°C during 60 h. Heating and cooling rates have been set at 1°C/min. The powders are then washed several times with water, filtered and rinsed with ethanol prior to be dried at 80°C in an oven for during 1h. Regarding the synthetic conditions (hydrothermal) and the subsequent washing using water several times, the products appear to be stable in water.

Scanning electron microscopy (SEM) analysis was performed with a FEI Technai G2 20 microscope operating at 200 kV.

X-ray powder diffraction (XRPD) analysis was performed at room temperature in a 2θ range of 10−120° with a scan step width of 0.02° using a D8 Advance A25 Bruker AXS diffractometer in Bragg−Brentano geometry equipped with a 1D LynxEye XE-T detector. Rietveld refinements were performed using Fullprof.[1] A highly crystalline LaB_6 (NIST SRM 660c) has been used to produce the instrumental resolution function file.

The thermogravimetric analysis (TGA) where conducted on a TGA-92 thermobalance (Setaram) under argon. The evolved gases were monitored by an Omnistar quadrupole mass spectrometer (MS, Pfeiffer) by continuously scanning in the range 0 – 100 amu. In order to control the atmosphere, the whole thermobalance was evacuated and filled with the carrier gas before heating up the samples up to 800 °C at a rate of 5 K/min.

IR - Fourier transform infrared spectra of the samples were recorded with a PerkinElmer spectrometer, between 4000 and 400 cm^{-1} with 4 cm^{-1} spectral resolution. For each spectrum, 10 scans were averaged taking air as a reference.

X-ray photoelectron spectroscopy (XPS) experiments were performed using an AXIS Ultra DLD Kratos spectrometer equipped with a monochromatized aluminum source (Al Kα= 1486.7 eV) and charge compensation gun. All binding energies were referenced to the C 1s core level at 285 eV. Simulation of the experimental photo peaks was carried out using a mixed Gaussian/Lorentzian peak fit procedure according to the software supplied by CasaXPS. Semiquantitative analysis accounted for a nonlinear Shirley background subtraction.

NMR - ^{19}F MAS NMR experiments were carried out using a Bruker Avance III 9.4 T (400 MHz for proton) spectrometer equipped with a 2.5 mm double resonance probe spinning at a frequency of ν_R=25 kHz. We used DEPTH sequence to remove the background signal[2] and the radio-frequency amplitude was ν_1=92 kHz. Spectra were recorded with an accumulation of 16 scans and a recovery delay of 100 s. The ^{19}F chemical shifts were referenced to CaF_2 at δ_{iso}=-107 ppm. The estimation of the NMR shift of fluorine in the 8b Wyckoff position has been done thanks to the superposition model developed by Bureau et al.[3] using the Na-F distances obtained from Rietveld refinement.

UV−vis diffuse reflectance spectra were collected at room temperature using a PerkinElmer Lambda 650 spectrophotometer in the 200−800 nm range. Before the measurement, the blank was measured using $BaSO_4$ (standard for 100% reflectance) in order to calibrate the device.

Photo-electrochemistry. Transient photocurrents measurements and Mott-Schottky plots were carried out using a potentiostat/galvanostat coupled with Electrochemical Impedance Spectroscopy (EIS) module (PGSTAT204 -FRA32M, Metrohm). The photoelectrochemical cell (MM-PEC 15mL single sided-Magnetic Mount, Redox.me®) is made up from the pyrochlore sample coated on an ITO glass (delta technologies, LTD) as the working electrode, immersed in an electrolyte of an aqueous solution of 0.1 M of Na_2SO_4 (pH = 6.6). A platinum electrode and a standard Ag/AgCl electrode were used as counter electrode and as a reference electrode, respectively. To form the working electrode, the crushed powder is added to a mixture of water and N,N-Dimethylformanmide (DMF) solvents with 1:1 ratio. The paste obtained is then deposited on the ITO/Glass substrate by the drop casting method and dried at 80°C during few minutes in order to obtain a uniform layer. All the measurements were controlled with the Nova2.0 software allowing to regulate the excitation wavelength of different LEDs with low spectral dispersions (450, 470, 505, 530, 590, 617, 627 and 655 nm) as well as the luminous flux (from 0 to 126 mW / cm²).

Density Functional Theory (DFT) calculation were carried out by employing the projector augmented wave (PAW)[4,5] method encoded in the Vienna ab initio simulation package (VASP)[6] and the generalized gradient approximation of Perdew, Burke and Ernzerhof[7] (PBE) for the exchange-correlation functionals. The calculations were carried out on the Ta- and Nb-phase using a similar ordering scenario in the reduced triclinic cell to simplify the construction of the models. Owing to the partially disordered character of the O/F distribution of the experimental structures, a particular anionic configuration has been picked up among the possible configurations. The chosen model implies all Na in NaO_5F_3 and all Nb/Ta in BO_5F environments corresponding to their average coordination. Geometry optimizations at fixed unit cell parameters were carried out using a plane wave energy cutoff of 550 eV and 30 *k* points in the irreducible Brillouin zone. It converged with residual Hellman-Feynman forces on the atoms smaller than 0.03 eV/Å. The relaxed structures were used to calculate accurate electronic structure. For the later, the plane wave cutoff energies of 550 eV and the threshold of self-consistent-field energy convergence of 10^{-6} eV were used, with 163 *k* points in the irreducible Brillouin Zone.

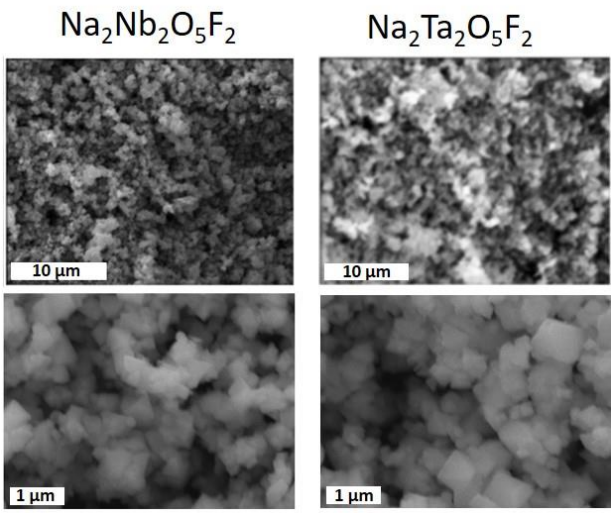

Figure S1: SEM images of $Na_2Nb_2O_5F_2$ and $Na_2Ta_2O_5F_2$.

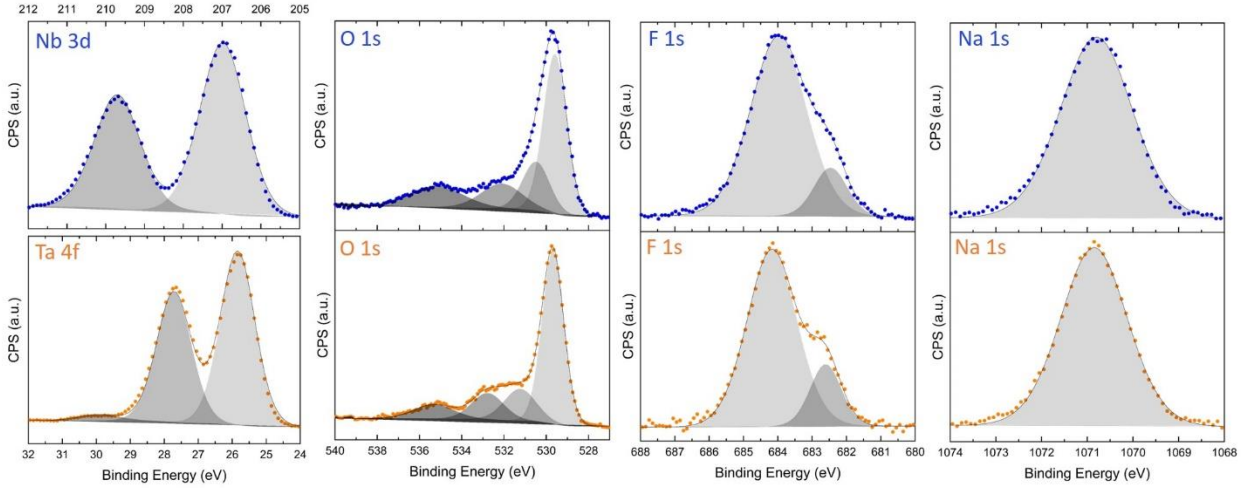

Figure S2: Fits of the XPS spectra of $Na_2Nb_2O_5F_2$ (blue, top panels) and $Na_2Ta_2O_5F_2$ (orange, bottom panels) at Na 1s, Nb 3d, Ta 4f, O 2p and F 1s core levels.

Table S1: details of binding energies (BE), FWHM, assignment and quantification obtained by fitting the data shown in the figure S2.

$Na_2Nb_2O_5F_2$				
Core level	Binding Energy (eV)	FWHM	Assignement	Relative surface atomic percentage [e]
Nb $3d_{5/2}$	207.0	1.4	Nb^{5+} [a]	18.0 %
Nb $3d_{3/2}$	209.7	1.4	Nb^{5+} [a]	
O 1s	529.6	1.3	Bulk O^{2-} [b]	46.8 %
O 1s	530.5	1.5	Surface O^{2-} [b]	
O 1s	532.1	2.3	Physisorbed water [b]	/
Na KLL	535.2	2.9	Na^+	/
F 1s	682.5	1.1	F^- [c]	18.0 %
F 1s	684.0	1.9	Ionic F^- [c]	
Na 1s	1070.8	1.9	Na^+ [d]	17.2 %
$Na_2Ta_2O_5F_2$				
Core level	Binding Energy (eV)	FWHM	Assignement	Relative surface atomic percentage [e]
Ta $4f_{7/2}$	25.8	1.2	Ta^{5+} [a]	17.7 %
Ta $4f_{5/2}$	27.7	1.2	Ta^{5+} [a]	
Na 2s	29.9	1.4	Na^+	/
O 1s	529.7	1.2	Bulk O^{2-} [b]	47.8 % [b]
O 1s	531.2	1.8	Surface O^{2-} [b]	
O 1s	532.8	2.2	Physisorbed water [b]	/
Na KLL	535.3	2.2	Na^+	/
F1s	682.6	1.1	F^- [c]	18.6 %
F 1s	684.2	1.7	Ionic F^- [c]	
Na 1s	1070.9	1.7	Na^+ [d]	15.9 %

(a) The Nb 3*d* doublet peak in $Na_2Nb_2O_5F_2$ and the Ta 4*f* doublet peak in $Na_2Ta_2O_5F_2$ have intensity ratios of 3:2 and 4:3 respectively with peak splitting of 2.74 and 1.91 eV, and are characteristics for Nb^{5+} and Ta^{5+} compounds.[8] Nb $3d_{5/2}$ binding energy (BE) is in between that of $NaNbO_3$ and K_2NbF_7 (BE (Nb $3d_{5/2}$, $NaNbO_3$) = 206.6 eV,[8] (BE (Nb $3d_{5/2}$, K_2NbF_7) = 209.4 eV[9]) and the Ta $4f_{7/2}$ BE is in between that of $NaTaO_3$ and K_2NbF_7 (BE (Ta $4f_{7/2}$, $NaTaO_3$) = 25.6 eV,[8] (BE (Ta $4f_{7/2}$, K_2TaF_7) = 29.4 eV[9]). This indicates intermediate iono-covalent characters - between oxide and fluoride - of the Ta/Nb-X bond of our pyrochlore compounds, in good agreement with the X site (48f Wyckoff position) being occupied by both O and F.

(b) For both materials, the BE of the bulk O^{2-} is similar to that observed for $NaNbO_3$ (BE (O 1s) = 529.7 eV)[8] and $NaTaO_3$ (BE (O 1s) = 530.0 eV)[8].

(c) The F 1s core level is composed of two contributions which could be assigned to fluorine in more or less ionic environment, in good agreement with F being located in both anionic sites of the structure.

(d) The Na 1s binding energy is very close to that observed in NaF.[10]

(e) The estimated surface compositions are $Na_{1.9}Nb_{2.0}O_{5.2}F_{2.0}$ and $Na_{1.8}Ta_{2.0}O_{5.4}F_{2.1}$

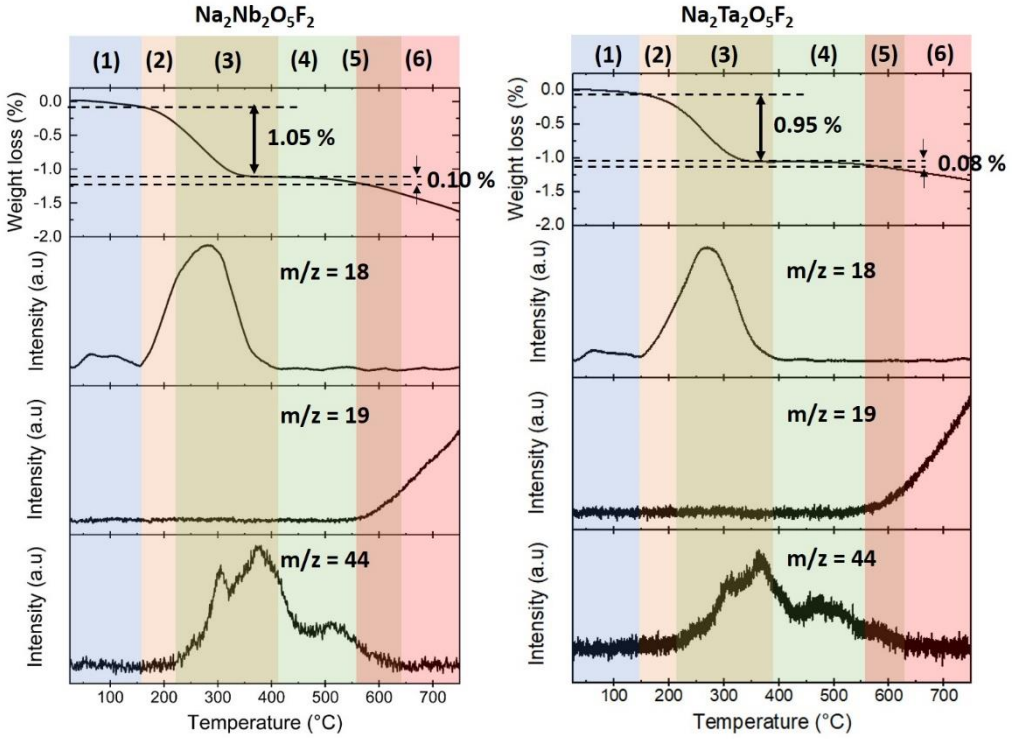

Figure S3: TGA-MS of $Na_2Nb_2O_5F_2$ and $Na_2Ta_2O_5F_2$ under Ar flow upon heating at 5K/min.

The TGA-MS trace of both materials can be divided into 6 regions:

Region (1) (*i.e.* 25-150 °C): adsorbed H_2O (m/z=18) is released alone.

Region (2) (*i.e.* 150-210 °C): intercalated H_2O (m/z=18) is released alone.

Region (3) (*i.e.* 210-400 °C): intercalated H_2O (m/z=18) and CO_2 (m/z=44) are released.

Region (4) (*i.e.* 400-560 °C): CO_2 (m/z=44) is released alone.

Region (5) (*i.e.* 560-640 °C): CO_2 (m/z=44) is released and F (m/z=19) are released.

Region (6) (*i.e.* 640-800 °C): F (m/z=19) is released alone.

As CO_2 is released together with H_2O in the region 3, it's required to deconvolute the corresponding mass losses in order to estimate the correct amount of intercalated H_3O^+ in the pyrochlore channel. In the region (4), CO_2 is released alone leading to a weight loss of 0.1% and 0.08% for $Na_2Nb_2O_5F_2$ and $Na_2Ta_2O_5F_2$. The integration of the CO_2 trace on the mass spectroscopy reveals that 30% (for $Na_2Nb_2O_5F_2$) and 45% (for $Na_2Ta_2O_5F_2$) of the total CO_2 signal is released in the region (4) and hence the weight losses associated with CO_2 during the region (3) is 0.3% and 0.1%. Consequently, it's possible to estimate that 0.75% and 0.86% of mass loss are associated with H_2O released over the whole temperature range and hence the compositions of our samples are estimated to be $Na_{1.9}(H_3O)_{0.1}Nb_2O_5F_2$ and $Na_{1.8}(H_3O)_{0.2}Ta_2O_5F_2$.

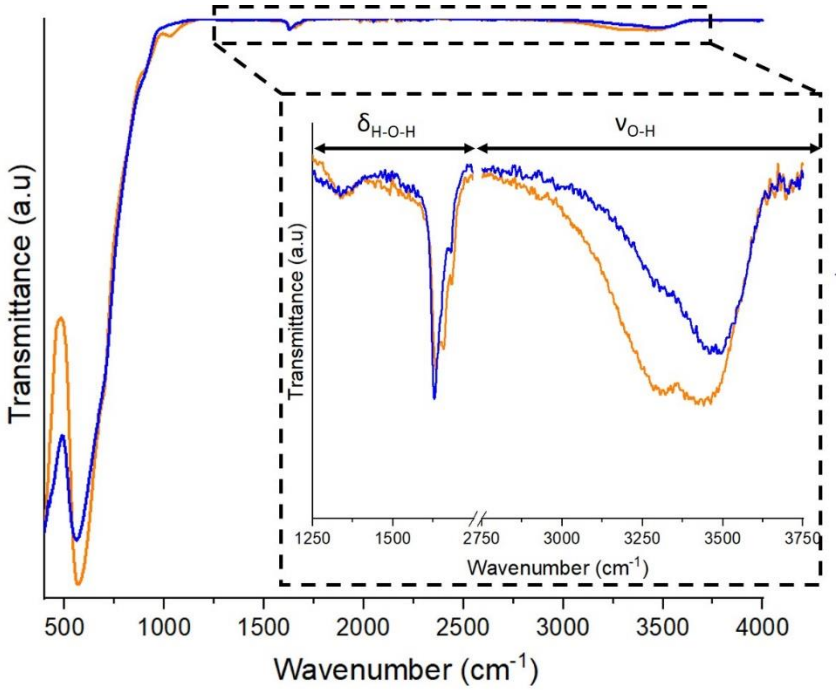

Figure S4: IR spectrum of $Na_2Nb_2O_5F_2$ (blue line) and $Na_2Ta_2O_5F_2$ (orange line)

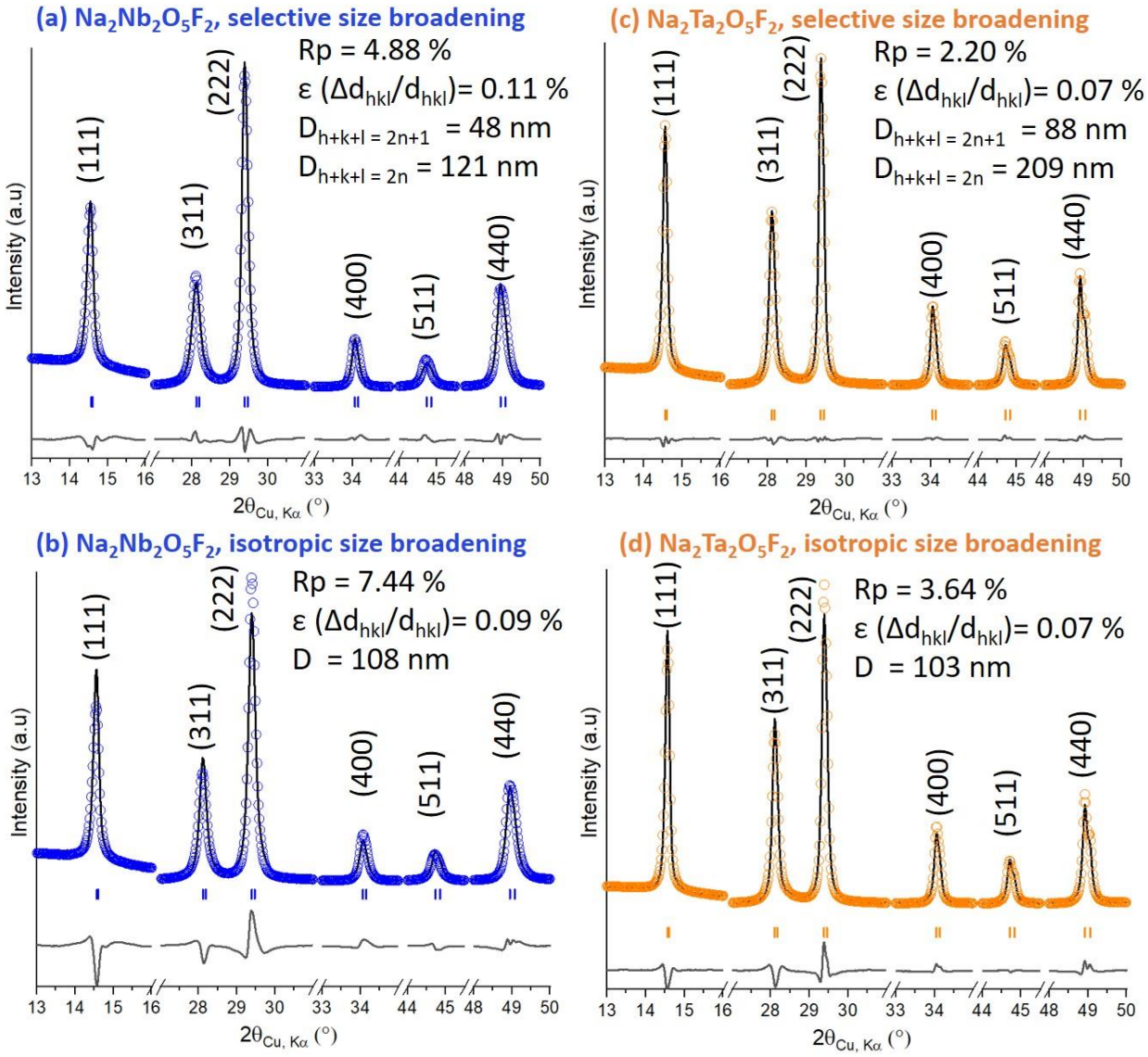

Figure S5: Lebail refinement of the profile of $Na_2Nb_2O_5F_2$ (a and b) and $Na_2Ta_2O_5F_2$ (c and d) using either a selective size broadening of the odd (h+k+l = 2n+1) reflection (a and c) or an isotropic size broadening model (b and d). For both materials, the agreement factors are better using the selective size broadening model. Indeed, the odd reflections appear to be broadened compared to the even Bragg peaks. This could be the signature of anti-phase boundary defects which could explain the shift of some odd reflections such as the (511) of $Na_2Nb_2O_5F_2$ which is badly fitted.[11]

Table S2: structural parameters obtained from Rietveld refinement of the structure of $Na_2Nb_2O_5F_2$ and $Na_2Ta_2O_5F_2$ based on XRPD data. The composition has been fixed to that estimated based on XPS and TGA.

$Na_2Nb_2O_5F_2$							
S.G.: *Fd-3m* Z = 8		*a* = 10.5181(3) Å				R_p = 4.99 % R_{wp} = 6.78 %	
atoms	Wyckoff position	*x*	*y*	*z*	Occupancy	U iso	BVS
Na	*16d*	½	½	½	0.95	0.045(3)	0.96(1)
OH_3	*16d*	½	½	½	0.05	0.045(3)	/
Nb	*16c*	0	0	0	1	0.028(1)	4.57(2)
O	*48f*	0.321(1)	⅛	⅛	0.833	0.042(3)	1.84(1)
F	*48f*	0.321(1)	⅛	⅛	0.167	0.042(3)	1.46(1)
F’	*8b*	⅜	⅜	⅜	1	0.032(3)	0.90(1)

$Na_2Ta_2O_2F_2$							
S.G.: *Fd-3m* Z = 8		*a* = 10.5231(1) Å				R_p = 2.44 % R_{wp} = 3.39 %	
Atoms	Wyckoff position	*x*	*y*	*z*	Occupancy	U iso	BVS
Na	*16d*	½	½	½	0.9	0.0154(4)	1.03(1)
OH_3	*16d*	½	½	½	0.1	0.0154(4)	/
Ta	*16c*	0	0	0	1	0.0113(3)	4.35(2)
O	*48f*	0.328(1)	⅛	⅛	0.833	0.0214(7)	1.80(1)
F	*48f*	0.328(1)	⅛	⅛	0.167	0.0214(7)	1.39(1)
F’	*8b*	⅜	⅜	⅜	1	0.0153(5)	0.90(1)

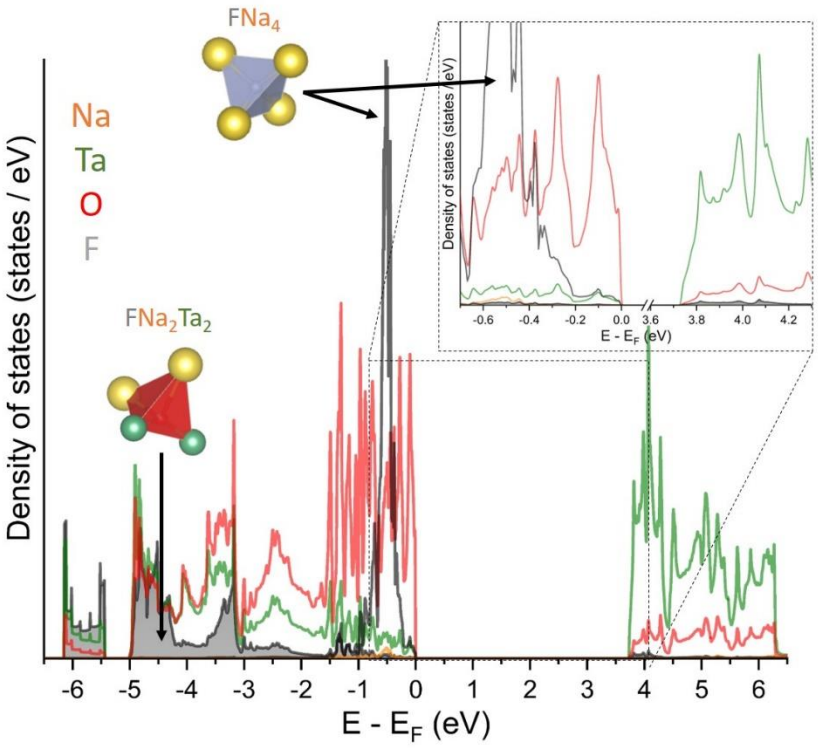

Figure S6: Projected Density of States (PDOS) of $Na_2Ta_2O_5F_2$. The Fermi level is set to zero.

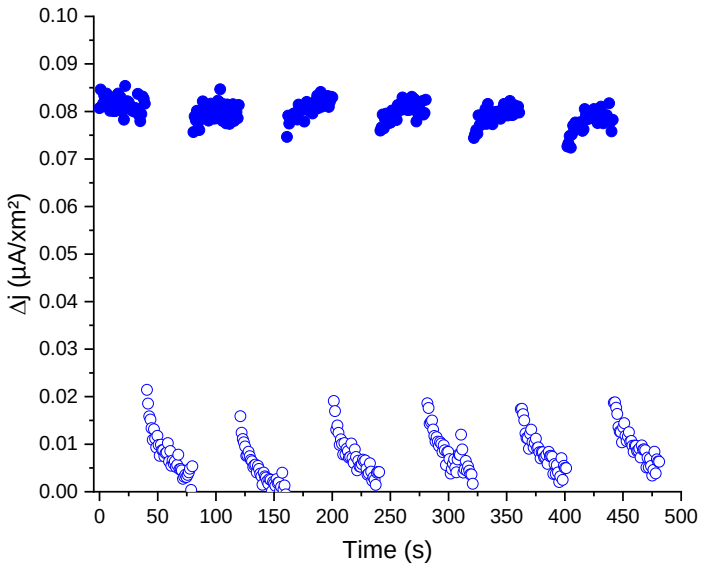

Figure S7. Photocurrent density stability *versus* time upon several successive cycles with light *on* and *off*. The measurements were carried out with a 450 nm wavelength source, with a light intensity of 42 mW/cm² and an applied potential V= 0.8 V.

References

(1) Rodriguez-carvajal, J. Recent Advances in Magnetic Structure Determination by Neutron Powder Diffraction. *Phys. B* **1993**, *192*, 55–69.

(2) Cory, D. G.; Ritchey, W. M. Suppression of Signals from the Probe in Nmr T1Measurements. *Spectrosc. Lett.* **1988**, *21* (7), 551–558.

(3) Bureau, B.; Silly, G.; Buzaré, J. Y.; Emery, J. Superposition Model for 19F Isotropic Chemical Shift in Ionic Fluorides: From Basic Metal Fluorides to Transition Metal Fluoride Glasses. *Chem. Phys.* **1999**, *249*, 89–104.

(4) Bloch, P. E. Projector Augmented-Wave Method. *Phys. Rev. B* **1994**, *50* (24), 17954–17979.

(5) Joubert, D. From Ultrasoft Pseudopotentials to the Projector Augmented-Wave Method. *Phys. Rev. B - Condens. Matter Mater. Phys.* **1999**, *59* (3), 1758–1775.

(6) Kresse, G.; Furthmüller, J. Efficiency of Ab-Initio Total Energy Calculations for Metals and Semiconductors Using a Plane-Wave Basis Set. *Comput. Mater. Sci.* **1996**, *6* (1), 15–50.

(7) Perdew, J. P.; Burke, K.; Ernzerhof, M. Generalized Gradient Approximation Made Simple. *Phys. Rev. Lett.* **1996**, *77* (18), 3865–3868.

(8) Ho, S. F.; Contarini, S.; Rabalais, J. W. Ion-Beam-Induced Chemical Changes in the Oxyanions (MO,,"-) and Oxides (MO,) Where M = Cr, Mo, W, V, Nb, and Ta. *J. Phys. Chem.* **1987**, *91* (18), 4779–4788.

(9) Mcguire, G. E.; Schweitzer, G. K.; Carlson, T. A. Study of Core Electron Binding Energies in Some Group Ilia, Vb, and VIb Compounds. *Inorg. Chem.* **1973**, *12* (10), 2450–2453.

(10) Morgan, W. E.; Van Wazer, J. R.; Stec, W. J. Inner-Orbital Photoelectron Spectroscopy of the Alkali Metal Halides, Perchlorates, Phosphates, and Pyrophosphates. *J. Am. Chem. Soc.* **1973**, *95* (3), 751–755.

(11) Lutterotti, L.; Gialanella, S. X-Ray Diffraction Characterization of Heavily Deformed Metallic Specimens. *Acta Mater.* **1998**, *46* (1), 101–110.